

CuIr₂Te₄: A Quasi-Two-Dimensional Ternary Telluride Chalcogenide Superconductor

Dong Yan^{1#}, Yijie Zeng^{2#}, Guohua Wang³, Yiyuan Liu⁴, Junjie Yin², Tay-Rong Chang^{5,6}, Hsin Lin⁷, Meng Wang², Jie Ma³, Shuang Jia⁴, Dao-Xin Yao^{2*}, Huixia Luo^{1*}

¹ *School of Material Science and Engineering, Key Lab of Polymer Composite & Functional Materials, Sun Yat-Sen University, No. 135, Xingang Xi Road, Guangzhou, 510275, P. R. China*

² *School of Physics, State Key Laboratory of Optoelectronic Materials and Technologies, Sun Yat-Sen University, No. 135, Xingang Xi Road, Guangzhou, 510275, P. R. China*

³ *Department of Physics and Astronomy, Shanghai Jiao Tong University, Shanghai 200240, China*

⁴ *Department of Physics, Peking University, Beijing, 100871, China*

⁵ *Department of Physics National Cheng Kung University Tainan 701, Taiwan*

⁶ *Center for Quantum Frontiers of Research and Technology (QFort), Tainan 701, Taiwan*

⁷ *Institute of Physics, Academia Sinica, Taipei 11529, Taiwan*

These two authors made equal contributions

*Corresponding author:

H.X. Luo, E-mail address: luohx7@mail.sysu.edu.cn;

D. X. Yao, E-mail address: yaodaoy@mail.sysu.edu.cn

ABSTRACT: Here we report the first observation of superconductivity in the AB_2X_4 -type ternary telluride CuIr_2Te_4 , which is synthesized by a solid-state method in an evacuated quartz jacket. It adopts a disordered trigonal structure with space group $P\bar{3}m1$ (No. 164), which embodies a two-dimensional (2D) IrTe_2 layers and intercalated by Cu between the layers. We use a combination of experimental and first principles calculation analysis to look insight into the structural and physical properties. CuIr_2Te_4 consistently exhibited a bulk superconductivity transition at 2.5 K in electrical resistivity, magnetic susceptibility and specific heat measurements. Resistivity and magnetization measurements suggest a charge density wave transition ($T_{CDW} \approx 250$ K) coexists in CuIr_2Te_4 , which further signify the coexistence of superconductivity and CDW in the ternary telluride chalcogenide CuIr_2Te_4 . Our discovery of the new CDW-bearing superconductor CuIr_2Te_4 opens a door for experimental and theoretical studies of the interplay between CDW and superconductivity quantum state in the condensed matter field.

KEYWORDS: CuIr_2Te_4 ; Superconductivity; AB_2X_4 family; Ternary telluride chalcogenide.

INTRODUCTION

The AB_2X_4 chalcogenide system ($A, B =$ transition metal ions; $X =$ S, Se, Te) have attracted continuous research interests due to their rich structure types and abundant physical properties.¹⁻⁵ The ternary and pseudo-ternary AB_2X_4 chalcogenides generally adopt the cubic spinel structure (space group $Fd\bar{3}m$), monoclinic defect NiAs structure (space group $I2/m$) or the disordered trigonal structure (space group $P\bar{3}m1$).⁶⁻⁸ Many AB_2X_4 -type ternary and pseudo-ternary sulfo- and seleno-spinels have been discovered in past decades, but there are few examples of superconducting spinels.⁹

CuV_2S_4 sulfo-spinel is one of the earliest three-dimensional AB_2X_4 -type materials known to superconduct ($T_c = 4.45$ - 3.20 K) and strikingly exhibits three charge-density wave (CDW) states ($T_{CDW1} = 55$ K, $T_{CDW2} = 75$ K, $T_{CDW3} = 90$ K).¹⁰⁻¹¹ The famous $CuRh_2S_4$ and $CuRh_2Se_4$ with the typical cubic spinel structure are also well known superconductors with $T_c = 4.35$ and 3.50 K, respectively.¹²⁻¹⁶ Yet, another popular ternary metal chalcogenide spinel compound, $CuIr_2S_4$, doesn't superconduct but exhibits a quite odd metal-insulator (M-I) transition at $T \approx 230$ K, which is followed by a complex structural transition that simultaneously produces both charge ordering and metal-metal pairing.¹⁷ Interesting, the M-I transition can be suppressed and dome-like superconductivity phase diagram ($T_c(x)$) was discovered by Zn substitution for Cu in the $Cu_{1-x}Zn_xIr_2S_4$ solid solution, with a maximum T_c of 3.4 K near $x = 0.3$.¹⁸ The other prototypical ternary metal seleno-chalcogenide $CuIr_2Se_4$ with the same spinel structure as $CuIr_2S_4$, remains metallic behavior from room temperature down to 0.5 K. Neither M-I or nor superconducting transitions are observed at ambient pressure, but a M-I transition is found above 2.8 GPa.¹⁹⁻²¹ Surprisingly, a superconductivity was observed in $Cu(Ir_{1-x}Pt_x)_2Se_4$ ($0.1 \leq x \leq 0.35$) with a maximum $T_c = 1.76$ K near $x = 0.2$ with Pt substitution for Ir in the $CuIr_{2-x}Pt_xSe_4$ solid solution.²² Despite hundreds of AB_2X_4 -type materials have been discovered, the superconductors found in this family are only the aforementioned CuV_2S_4 , $CuRh_2S_4$, $CuRh_2Se_4$, electron-doped $CuIr_2S_4$ and electron-doped $CuIr_2Se_4$ sulfo- or seleno- spinels. All of the above mentioned superconducting AB_2X_4 -type compounds have the normal spinel structure where the Cu

ions occupy the A tetrahedral sites and the transition metal ions (V, Rh, Ir) occupy the B octahedral sites. To the best of our knowledge, no superconductivity has been observed in AB_2X_4 -type telluro-compounds or AB_2X_4 -type sulpho- and seleno-compounds with defect structures related to NiAs so far.

Currently, it is commonly approved that low dimensionality leads to particular electronic structures and allows relatively strong fluctuations, which may improve superconductivity. Although CDW sometimes contests with superconductivity, mainly in the quasi-one-dimensional case.²³ From a crystal-chemistry perspective, low-dimensional structures easily appear in inorganic metal compound with relatively high polarizability and low electronegativity anions. For instance, by comparison with metal oxides, metal chalcogenides have a tendency to crystallize in layered structures,²⁴⁻²⁵ which leads to rich and interesting physical phenomena such as CDW and superconductivity.^{23,26} Thus, it is wise to search for new superconductors in the AB_2X_4 -type chalcogenides with low-dimensional crystal structures. On the other hand, among chalcogenides, the crystal structures electronic structures and physical properties of tellurides are often different from sulfides and selenides, since Te has the largest ionic radius among S, Se and Te. About two decades ago, Nagata et al. observed anomalies in resistivity and magnetic susceptibility in $CuIr_2Te_4$, probably resulting from the formation of CDW.²⁷ However, its low-temperature properties have not been characterized. Unlike $CuIr_2S_4$ and $CuIr_2Se_4$ spinels, $CuIr_2Te_4$ crystallizes in a two-dimensional (2D) disordered trigonal structure with the space group $P-3m1$ at room temperature, which embodies a complicated 2D $IrTe_2$ layers and intercalated by Cu between the layers (**Figure 1a**). On first sight though no superconducting transition was observed from ambient temperature down to 4.2 K, it seems to be an ordinary metal with a CDW transition around 250 K. Only limited reports have been given by earlier researchers, and no complete studies and analysis related with superconductivity are yet explored. However, it is well-known that many of the two-dimensional dimensional transition metal dichalcogenides (TMDCs) exhibit CDW and some of them displays the competition/coexistence between CDW and superconductivity. Inspired by the 2D TMDCs, we quested for the coexistence of CDW and superconductivity in the 2D

ternary telluride chalcogenide CuIr_2Te_4 of AB_2X_4 type.

In the present contribution, we report the first observation of superconductivity in AB_2X_4 -type ternary telluride CuIr_2Te_4 , which was successfully synthesized through solid-state reaction method. The structural properties of the AB_2X_4 -type telluro-compound CuIr_2Te_4 was characterized via X-ray diffraction (XRD), energy dispersive X-ray spectrometer (EDXS) and high-resolution transmission electron microscopy (HRTEM). Meanwhile, the superconductivity properties were systematically studied *via* combining with experimental and first principles calculation analysis. The results of magnetization, resistivity, and heat capacity measurements demonstrate that CuIr_2Te_4 is a quasi-two-dimensional ternary telluride chalcogenide superconductor with $T_c \approx 2.5$ K and suggest that a CDW state emerges below around 250 K. With the discovery of this CDW-bearing superconductor CuIr_2Te_4 , there is large room for further explorations of the interplay between CDW and superconductivity in the AB_2X_4 system.

EXPERIMENTAL

Method and materials

Polycrystalline CuIr_2Te_4 was prepared by a conventional solid-state reaction method. Mixtures of high-purity fine powders of Cu (99.5%), Ir (99.95%) and Te (99.999%) in the appropriate stoichiometric ratios were thoroughly ground, pelletized and heated in a sealed quartz tube at 850 °C for 96 h. Subsequently, the as-prepared powders were reground, pelletized and sintered at 900 °C for 96 h.

We also adopted the powder X-ray diffraction (PXRD, Bruker D8 focus, Cu $K\alpha$ radiation, graphite diffracted beam monochromator) to characterize the samples structurally. The unit cell parameters were determined by profile fitting the powder diffraction data with FULLPROF diffraction suite with Thompson-Cox-Hastings pseudo-Voigt peak shapes.²⁸ A Quantum Design Physical Property Measurement System (PPMS) was used to take the measurements of the temperature dependence of electrical resistivity and heat capacity from 2 K to 300 K. No materials' air-sensitivity was found during the measurements. T_c determined from the susceptibility data were estimated conservatively: T_c was taken as the intersection of the extrapolations of the

steepest slope of the susceptibility in the superconducting transition region and the normal state susceptibility; T_c was determined from the midpoint of the resistivity $\rho(T)$ transitions for the resistivity data; for the specific heat data, we employed equal area construction method to obtain the critical temperature.

The microscopic morphology and the composition of CuIr_2Te_4 sample were investigated by scanning electron microscopy (SEM, Quanta 400F, Oxford) and energy dispersive X-ray spectroscopy (EDXS), respectively. And high-resolution transmission electron microscopy (HRTEM, FEI Tecnai G2 F20 operated on 200 kV) was used to study the phase structure of CuIr_2Te_4 .

Calculational Details

The first principles calculation was carried out by using the projector augmented wave method²⁹ implemented in the VASP package.³⁰ The generalized gradient approximation suggested by Perdew, Burke and Ernzerhof³¹ was used for the exchange-correlation interaction. The cutoff energy was set to 900 eV and a Monkhorst-Pack grid³² of $15 \times 15 \times 11$ was used for k -point sampling. The spin-orbit coupling was considered in the band structure calculation.

Phonon dispersion was calculated by finite displacement method as implemented in Phonopy³³, with a supercell of $3 \times 3 \times 2$. Since the occupation of Cu is 0.5 at $1b$ site (see **Table 1**), we built the primitive unit cell by doubling the unit cell of $P\bar{3}m1$ along c and preserved only one Cu atom. Physically this corresponds to the case that Cu was intercalated by every two IrTe_2 layers. We will see this is a reasonable model as it gives results in agreement with experiment semi-quantitatively.

RESULTS AND DISCUSSION

Figure 1 shows powder XRD characterization for polycrystalline CuIr_2Te_4 . Except for tiny impurities of Ir, all the reflection peaks can be indexed to the CuIr_2Te_4 compound, which adapts to the disordered trigonal structure with the space group $P\bar{3}m1$ at room temperature. CuIr_2Te_4 exhibits a two-dimensional disordered trigonal structure, which embodies two-dimensional (2D) IrTe_2 layers intercalated by Cu between the

layers. (**Figure 1a**). The lattice parameters are obtained to be $a = b = 3.9397(3)$ Å and $c = 5.3964(6)$ Å (**Table 1**). **Figure 1d** is the scan electron microscope (SEM) images of the CuIr_2Te_4 polycrystalline powder sample, which signify CuIr_2Te_4 has a layer structure. The HRTEM image (**Figure 1b**) of CuIr_2Te_4 polycrystalline powder shows clear lattice distance of 0.510 nm. Fast Fourier transform images (FFT) are shown in the upper right corner of the image. **Figure 1c** shows the [001] zone axis pattern (ZAP) of CuIr_2Te_4 . It indicates that CuIr_2Te_4 has a trigonal structure; which is consistent with the XRD data previously mentioned. The EDXS spectrum (**Figure 1e**) shows three elements of Cu, Ir and Te in the as-prepared CuIr_2Te_4 polycrystalline powder sample. And the element ratio of Cu, Ir and Te is close to 1: 1.9: 4, indicating that the CuIr_2Te_4 polycrystalline powder compound is close to stoichiometric ratio.

The cooling and warming temperature dependence of electrical resistivity ($\rho(T)$) for polycrystalline CuIr_2Te_4 under zero magnetic field is shown in the main panel of **Figure 2a**. The samples show a metallic temperature dependence ($d\rho/dT$) in the region of 2.7 to 300 K. The up-left corner inset of **Figure 2a** presents the $d\rho/dT$ vs. T curve at low temperature, which further confirms the T_c is around 2.5 K. A sharp drop of $\rho(T)$ obviously takes place below 2.7 K (bottom right corner inset of **Figure 2a**), which represents the occurrence of superconductivity and demonstrates the details of the superconducting transition. Superconductivity is also confirmed by the zero-field-cooled (ZFC) and field-cooled (FC) dc magnetic susceptibility measurements (**Figure 2b**), showing a strong diamagnetism below 2.5 K. The superconducting volume fraction can be estimated approximately to be 96.4 %, which reveals the high purity of the CuIr_2Te_4 sample. The inset of **Figure 2b** shows the $d\chi/dT$ vs T curve at low temperature, revealing a sharp peak at the superconducting transition temperature. As shown in **Figure 2c**, the susceptibility exhibits an anomaly around 250 K with the hysteresis, which indicate the CDW transition at around 250 K and is in consistent with the previous report.²⁷ Inset of **Figure 2c** shows the measured temperature range from 150 to 300 K of electrical resistivity ($\rho(T)$) at applied field in the range from 0 to 9 T with cooling and heating. Resistivity measurements all exhibited a distinct phase transition associated with the formation of CDW around 225 - 300 K, which was not affected by

the applied magnetic fields. The above results reveal that CuIr_2Te_4 is a new CDW-bearing superconductor.

Temperature-dependent measurements of the magnetization under incremental magnetic field $M(H)$ were applied to determine the upper critical field $\mu_0 H_{c1}(0)$. **Figure 2d** shows how the $\mu_0 H_{c1}(0)$ for CuIr_2Te_4 was determined. First, applied field magnetization measurements $M(H)$ were performed at 1.8, 2.0, and 2.2 K to calculate the demagnetization factor (N). With the hypothesis that the beginning linear response to the magnetic field is perfectly diamagnetic ($dM/dH = -1/4 \pi$) for this bulk superconductor, we obtained the values of demagnetization factor N , of 0.1 – 0.592 (from $N = 1/4\pi\chi_V + 1$), where $\chi_V = dM/dH$ is the value of linearly fitted slope for the up-right corner inset of **Figure 2d**. The experimental data can be fitted with the formula $M_{\text{fit}} = a + bH$ at low magnetic fields, where a is an intercept and b is a slope from fitting the low magnetic field magnetization measurements data. The bottom left corner inset of **Figure 2d** shows the $M(H) - M_{\text{fit}}$ data versus the magnetic field(H). $\mu_0 H_{c1}^*$ was determined at the field when M deviates by $\sim 1\%$ above the fitted data (M_{fit}), as is the common practice.³⁵ We can obtain the lower critical field $\mu_0 H_{c1}(T)$ in the consideration of the demagnetization factor (N), *via* the formula $\mu_0 H_{c1}(T) = \mu_0 H_{c1}^*(T) / (1 - N)$.³⁶⁻³⁷ The main panel of **Figure 2d** reveals the $\mu_0 H_{c1}(T)$ as the function of temperature for CuIr_2Te_4 . We estimated the $\mu_0 H_{c1}(0)$ by fitting the $\mu_0 H_{c1}(T)$ data *via* the formula $\mu_0 H_{c1}(T) = \mu_0 H_{c1}(0) [1 - (T/T_c)^2]$, which was shown by the black solid lines. The obtained zero-temperature lower critical field $\mu_0 H_{c1}(0)$ for CuIr_2Te_4 was 0.028(2) T (**Table 2**).

With the purpose of estimating the critical field $\mu_0 H_{c2}(0)$, we examined temperature dependent electrical resistivity at various applied fields $\rho(T, H)$ for CuIr_2Te_4 sample. **Figure 2e** exhibits the $\rho(T, H)$ measurement data for CuIr_2Te_4 . **Figs. 2f** shows upper critical field values $\mu_0 H_{c2}$ plotted *vs* temperature with T_c s obtained from resistivity at different applied fields. The $\mu_0 H_{c2}$ *vs* T curve near T_c of CuIr_2Te_4 sample shows the well linearly fitting, which is represented by solid line. The value of fitting data slope (dH_{c2}/dT) of CuIr_2Te_4 sample was shown in **Table 2**. We can estimate the zero-temperature upper critical field (**Figure 2f**) of 0.12 T for CuIr_2Te_4 from the data, using the Werthamer-Helfand-Hohenberg (WHH) expression formula $\mu_0 H_{c2} = -0.693 T_c$

(dH_{c2}/dT_c) for the dirty limit superconductivity.³⁸⁻⁴² This obtained result was also summarized in **Table 2**. The Pauli limiting field of CuIr_2Te_4 was calculated from $\mu_0 H^P = 1.86T_c$. The calculated values of $\mu_0 H^P$ was larger than the estimated values. Then, with this formula $\mu_0 H_{c2} = \frac{\phi_0}{2\pi\xi_{\text{GL}}^2}$, where ϕ_0 is the flux quantum, the Ginzburg-Landau coherence length ($\xi_{\text{GL}}(0)$) was calculated ~ 52.8 nm for CuIr_2Te_4 (**Table 2**).

For the sake of getting more abundant information of the electronic and superconducting properties of CuIr_2Te_4 polycrystalline sample, we took the heat capacity measurements for the polycrystalline sample under 0 T and 3 T applied magnetic field. The obtained T_c from heat capacity matched the T_c obtained by the $\chi(T)$ and $\rho(T)$ measurements well, which provides convincing evidence that a bulk superconducting state is achieved in CuIr_2Te_4 . Thus, we have found a new layered quasi-two-dimensional ternary telluride AB_2X_4 chalcogenide superconductor wherein a superconducting state competes with CDW state, akin to the two-dimensional transition metal dichalcogenides (TMDCs). By fitting the normal state data of specific heats at high temperature under 3 T magnetic field, it is found to obey the formula $C_p = \gamma T + \beta T^3$, where γ and β describe the electronic and phonon contributions to the heat capacity, respectively.

We got the values of γ and β (inset of **Figure 5**) from fitting the data got under 3 T applied field in temperature range of 4 – 10 K. The normalized specific heat jump value $\Delta C/\gamma T_c$ obtained from the data (**Figure 3a**) was 1.82 for CuIr_2Te_4 , which was much higher than the Bardeen-Cooper-Schrieffer (BCS) weak-coupling limit value (1.43), confirming bulk superconductivity.

Then we obtain the Debye temperature by the formula $\Theta_D = (12\pi^4 nR/5\beta)^{1/3}$ by using the fitted value of β , where n is the number of atoms per formula unit and R is the gas constant. Thus, we can estimate the electron-phonon coupling constant (λ_{ep}) by using the Debye temperature (Θ_D) and critical temperature T_c from the inverted

McMillan formula: $\lambda_{ep} = \frac{1.04 + \mu^* \ln\left(\frac{\Theta_D}{1.45T_c}\right)}{(1 - 1.62\mu^*) \ln\left(\frac{\Theta_D}{1.45T_c}\right) - 1.04}$.³⁸ This resultant λ_{ep} is 0.65, suggesting

that CuIr_2Te_4 belongs to an intermediately coupled superconductor. The electron

density of states at the Fermi level ($N(E_F)$) can be calculated from $N(E_F) = \frac{3}{\pi^2 k_B^2 (1 + \lambda_{ep})} \gamma$ with the γ and λ_{ep} . This yields a value that $N(E_F) = 2.72$ states/eV f.u. for CuIr_2Te_4 (**Table 2**). The superconducting parameters of CuIr_2Te_4 are summarized in **Table 2**, and have a comparison with those sulpho- or seleno- spinels superconductors.

We now turn to the calculated electronic property of CuIr_2Te_4 in the disordered trigonal structure. The optimized structure of our model shows the interlayer distances between IrTe_2 layers are 5.21 Å and 5.60 Å, in the presence and absence of Cu intercalation, respectively. The former is close to that of 5.1 Å seen in **Figure 1** (b). Compared with pure IrTe_2 with $c = 5.3984$ Å,⁴³ the intercalation of Cu tends to reduce the interlayer distance (**Table 1**), and the interlayer Te-Te bonding⁴⁴ is expected to be stronger. This can be seen from the band structure, as shown in **Figure 4**, where the bands disperse strongly along ΓA . As revealed by both orbital projected band structure and density of state, the bands near the Fermi energy E_F mainly come from Te p and Ir d orbitals, similar to that of CuIr_2S_4 in spinel structure.⁴⁶ Moreover, note that the density of states at the Fermi energy is 1.65, smaller than the experimentally derived value. Since the element ratio of Cu, Ir and Te is close to 1: 1.9: 4 in our sample, the 0.1 Ir vacancy can be thought of hole doping, thus the experimental value corresponds to the density of states at somewhere below the Fermi energy (~ 0.1 eV), which agrees better with the calculated result. Furthermore, one can notice that the Fermi energy locates at a flat plateau, not a local maximum, in the density of states. This behavior is also seen in CuRh_2S_4 ⁴⁶, CuV_2S_4 ⁴⁷ and monolayer NbSe_2 ⁴⁸. Although the structure of the CDW phase is still unknown, the change of density of states due to CDW transition is expected to be small,⁴³ and our comparison between the experimental and calculated values is reasonable.

Figure 5 shows the Fermi surface, which consists of two parts, the outer Fermi surface is flower-like and the inner one is vase-like. Inside the inner Fermi surface, there is another egg-like Fermi surface surrounding Γ not seen in the figure. The shape of the two Fermi surfaces varies along ΓA , and remarkable nesting effects of the Fermi surface should not be expected.⁴⁶ Spin polarized calculation was further performed to

confirm that no magnetism appears, and the rising behavior of magnetic susceptibility at low temperature (**Figure 2c**) was not from splitting of bands due to spin polarization under magnetic field. Compared with *Ref. 27*, where the magnetic susceptibility satisfies the Curie-Weiss law, our data here is more complicated in that the susceptibility remains nearly constant in the temperature range of 50 – 200 K, and can't be described solely by the Pauli paramagnetism. Since no magnetism appears, the spin fluctuation due to the divergence of spin susceptibility

$$\chi^s(\mathbf{q}, i\omega_n)=[1-\chi^0(\mathbf{q}, i\omega_n)U]^{-1}\chi^0(\mathbf{q}, i\omega_n)$$

does not play a role, where $\chi^s(\mathbf{q}, i\omega_n)$, $\chi^0(\mathbf{q}, i\omega_n)$ are the spin susceptibility with and without correlation U , respectively. Therefore, the superconducting transition temperature should be low, as what is found here.⁴⁹ To see the origin of the CDW phase we calculated the phonon dispersion of CuIr_2Te_4 (**Figure 6**). As can be seen, neither imaginary branches nor unusual discontinuity dip can be found, suggesting that the CDW is not driven by Kohn anomaly⁴⁵ similar to pure IrTe_2 .⁴³ Since the wave vector characterizing the CDW phase is not determined in our work, the superlattice corresponding to CDW is thus unknown.

However, the resistivity anomaly near around 250 K shows CDW character. With the evidence we have, the sudden rise in resistivity at 250 K, as temperature is lowered, is expected to come from the reduced density of states at Fermi energy. We suspect this reduced density of state is due to a sudden increase in the correlation between Ir d electrons during their hopping process, as temperature is lowered. At low temperature the frequency disperses linearly with the wave vector, and the heat capacity due to phonon part varies linearly with T^3 . We deduced the coefficient to be 1.77, as shown in Figure 3b. The deduced Debye temperature is 197.36 K, agrees well with the experimentally derived value.

CONCLUSION

Here we report the first observation of the coexistence of the superconductivity and charge density wave in the AB_2X_4 -type ternary telluride CuIr_2Te_4 , which was

synthesized *via* a solid-state reaction method. From the results of magnetization, resistivity and heat capacity measurements we find that CuIr_2Te_4 is a quasi-two-dimensional ternary telluride chalcogenide superconductor with a $T_c \approx 2.5$ K and coexists a CDW state around 250 K. Electronic structure calculation shows the states near the Fermi energy mainly come from Te p and Ir d orbitals. The lack of nesting in the Fermi surface and the missing of unusual discontinuity in phonon spectrum exclude the possibility that the CDW phase is driven by Fermi surface nesting and Kohn anomaly, respectively. Moreover, the calculated density of states at Fermi energy, phonon part of heat capacity at low temperature, and Debye temperature agrees semi-quantitatively with the experimental values, confirming the validity of our model. From more profound experimental and theoretical study CDW-bearing superconductor like CuIr_2Te_4 , we can clarify the interplay between CDW and superconductivity quantum state hopefully in the condensed matter field.

ACKNOWLEDGMENT

The authors thank R. Cava, B. Shen and W.W. Xie for valuable discussions. H. X. Luo acknowledges the financial support by “Hundred Talents Program” of the Sun Yat-Sen University and Natural Science Foundation of China (21701197). J. Ma is supported by the National Natural Science Foundation of China (Grant No. 11774223). Y. Zeng and D. X. Yao are supported by NKRDPC Grants No. 2017YFA0206203, No. 2018YFA0306001, NSFC-11574404, National Supercomputer Center in Guangzhou, and Leading Talent Program of Guangdong Special Projects. T.-R.C. was supported by the Young Scholar Fellowship Program from the Ministry of Science and Technology (MOST) in Taiwan, under a MOST grant for the Columbus Program MOST108-2636-M-006-002, National Cheng Kung University, Taiwan, and National Center for Theoretical Sciences, Taiwan. This work was supported partially by the MOST, Taiwan, Grant MOST107-2627-E-006-001. This research was supported in part by Higher Education Sprout Project, Ministry of Education to the Headquarters of University Advancement at National Cheng Kung University (NCKU).

REFERENCES

- (1) Lotgering, F. K. On the ferrimagnetism of some sulphides and oxides. *Philips Res. Rep.* 1956, 11, 190.
- (2) Nagata, S.; Hagino, T.; Seki, Y.; Bitoh, T. Metal-insulator transition in thiospinel CuIr_2S_4 . *Physica B* 1994, 194, 1077-1078.
- (3) Radaelli, P. G.; Horibe, Y.; Gutmann, M. J.; Ishibashi, H.; Chen, C. H.; Ibberson, R. M.; Koyama, Y.; Hor, Y. S.; Kiryukhin, V.; Cheong, S. W. Formation of isomorphous Ir^{3+} and Ir^{4+} octamers and spin dimerization in the spinel CuIr_2S_4 . *Nature* 2002, 416, 155-158.
- (4) Hagino, T.; Seki, Y.; Wada, N.; Tsuji, S.; Shirane, T.; Kumagai, K. I.; Nagata, S. Superconductivity in spinel-type compounds CuRh_2S_4 and CuRh_2Se_4 . *Phys. Rev. B* 1995, 51, 12673.
- (5) Ito, M.; Taira, A.; Sonoda, K. Superconducting Parameters of Spinel CuRh_2S_4 under Pressure. *Acta Physica Polonica A.* 2017, 131, 1450-1453.
- (6) Plovnick, R. H.; Vlasse, M.; Wold, A. Preparation and Structural Properties of Some Ternary Chalcogenides of Titanium. *Inorg. Chem.* 1968, 7, 127-129.
- (7) Holt, S. L.; Bouchard, R. J.; Wold, A. Ternary chalcogenides of vanadium and chromium. *J. Phys. Chem. Solids* 1966, 27, 757-759.
- (8) Plovnick, R. H.; Perloff, D. S.; Vlasse, M.; Wold, A. Electrical and structural properties of some ternary chalcogenides of titanium. *J. Phys. Chem. Solids* 1968, 29, 1935-1940.
- (9) Van Maaren, N. H.; Schaeffer, G. M.; Lotgering, F. K. Superconductivity in sulpho- and selenospinels. *Phys. Lett. A* 1967, 25, 238-239.
- (10) Fleming, R. M.; DiSalvo, F. J.; Cava, R. J.; Waszczak, J. V. Observation of charge-density waves in the cubic spinel structure CuV_2S_4 . *Phys. Rev. B* 1981, 24, 2850-2853.
- (11) Nagard, N. L.; Katty, A.; Collin, G.; Gorochoy, O.; Willig, A. Preparation, crystal structure and physical properties (transport, magnetic susceptibility and NMR) of CuV_2S_4 spinel. *J. Solid State Chem.* 1979, 27, 267-277.
- (12) Robbins, M.; Willens, R. H.; Miller, R. C. Superconductivity in the spinels

- CuRh₂S₄ and CuRh₂Se₄. *Solid State Commun.* 1967, 5, 933-934.
- (13) Lotgering, F. K.; Van Stapele, R. P. Magnetic Properties and Electrical Conduction of Copper-Containing Sulfo- and Selenospinel. *J. Appl. Phys.* 1968, 39, 417-423.
- (14) Lotgering, F. K. Magnetic and electrical properties of Co_{1-x}Cu_xRh₂S₄. *J. Phys. Chem. Solids* 1969, 30, 1429-1434.
- (15) DiSalvo, F. J.; Waszczak, J. V. Magnetic properties of copper chalcogenide spinels. *Phys. Rev. B* 1982, 26, 2501-2506.
- (16) Shelton, R. N.; Johnston, D. C.; Adrian, H. Measurement of the pressure dependence of T_c for superconducting spinel compounds. *Solid State Commun.* 1976, 20, 1077-1080.
- (17) Wang, N. L.; Cao, G. H.; Zheng, P.; Li, G.; Fang, Z.; Xiang, T.; Kitazawa, H.; Matsumoto, T. Optical study of the metal-insulator transition in CuIr₂S₄ crystals. *Phys. Rev. B* 2004, 69, 153104.
- (18) Suzuki, H.; Furubayashi, T.; Cao, G.; Kitazawa, H.; Kamimura, A.; Hirata, K.; Matsumoto, T. Metal-Insulator Transition and Superconductivity in Spinel-Type System Cu_{1-x}Zn_xIr₂S₄. *J. Phys. Soc. Jpn.* 1999, 68, 2495-2497.
- (19) Chen, L.; Matsunami, M.; Nanba, T.; Matsumoto, T.; Nagata, S.; Ikemoto, Y.; Moriwaki, T.; Hirono, T.; Kimura, H. Far-infrared spectroscopy of electronic states of CuIr₂Se₄ at high pressure. *J. Phys. Soc. Jpn.* 2005, 74, 1099-1102.
- (20) Irizawa, A.; Kobayashi, M.; Satoh, K.; Nanba, T.; Chen, L.; Matsumoto, T.; Matsunami, M.; Ito, M.; Suzuki, T.; Nagata, S. Study on Cross-over Change from Metal to Insulator in the Electronic States of Copper-spinel Compounds under High Pressure. *J. Phys. Soc. Jpn.* 2007, 76, 13-14.
- (21) Furubayashi, T.; Kosaka, T.; Tang, J.; Matsumoto, T.; Kato, Y.; Nagata, S. Pressure induced metal-insulator transition of selenospinel CuIr₂Se₄. *J. Phys. Soc. Jpn.* 1997, 66, 1563-1564.
- (22) Luo, H. X.; Klimczuk, T.; Muehler, L.; Schoop, L.; Hirai, D.; Fucillo, M. K.; Felser, C.; Cava, R. J. Superconductivity in the Cu(Ir_{1-x}Pt_x)₂Se₄ spinel. *Phys. Rev. B* 2013, 87, 214510.
- (23) Smaalen, S. V. The Peierls transition in low-dimensional electronic crystals. *Acta*

- Crystallogr.* 2005, A61, 51-61.
- (24) Pell, M. A.; Ibers, J. A. Layered Ternary and Quaternary Metal Chalcogenides *Chem. Ber./Recueil* 1997, 130, 1-8.
- (25) Mitchell, K.; Ibers, J. A. Rare-Earth Transition-Metal Chalcogenides. *Chem. Rev.* 2002, 102, 1929-1952.
- (26) Wilson, J. A.; Disalvo, F. J.; Mahajan, S. Charge-density waves and superlattices in the metallic layered transition metal dichalcogenides. *Adv. Phys.* 1975, 24, 117-201.
- (27) Nagata, S.; Kijima, N.; Ikeda, S.; Matsumoto, N.; Endoh, R.; Chikazawa, S.; Shimono, I.; Nishihara, H. Resistance anomaly in CuIr_2Te_4 . *J Phys. Chem. Solids* 1999, 60, 163-165.
- (28) Rodríguez-Carvajal, J. FULLPROF: A Program for Rietveld Refinement and Pattern Matching Analysis. *Comm. Powder Diffr.* 2001, 26, 12-70.
- (29) Blöchl, P. E. Projector augmented-wave method. *Phys. Rev. B* 1994, 50, 17953-17979.
- (30) Kresse, G.; Joubert, D. From ultrasoft pseudopotentials to the projector augmented-wave method. *Phys. Rev. B* 1999, 59, 1758-1775.
- (31) Perdew, J. P.; Burke, K.; Ernzerhof, M. Generalized Gradient Approximation Made Simple. *Phys. Rev. Lett.* 1996, 77, 3865-3868.
- (32) Monkhorst, H. J.; Pack, J. D. Special points for Brillouin-zone integrations. *Phys. Rev. B* 1976, 13, 5188-5192.
- (33) Togo, A.; Tanaka, I. First principles phonon calculations in materials science. *Scripta Mater.* 2015, 108, 1-5.
- (34) Moshopoulou, E. G. Superconductivity in the spinel compound LiTi_2O_4 . *J. Am. Ceram. Soc.* 1999, 82, 3317-3320.
- (35) Luo, H. X.; Xie, W. W.; Tao, J.; Pletikosic, I.; Valla, T. G.; Sa-hasrabudhe, S.; Osterhoudt, G.; Sutton, E.; Burch, K. S.; Seibel, E. M.; Krizan, J. W.; Zhu, Y. M.; Cava, R. J. Differences in Chemical Doping Matter: Superconductivity in $\text{Ti}_{1-x}\text{Ta}_x\text{Se}_2$ but Not in $\text{Ti}_{1-x}\text{Nb}_x\text{Se}_2$. *Chem. Mater.* 2016, 28, 1927-1935.
- (36) Winiarski, M. J.; Wiendlocha, B.; Gołab, S.; Kushwaha, S. K.; Wiśniewski, P.; Kaczorowski, D.; Thompson, J. D.; Cava, R. J.; Klimczuk, T. Superconductivity in

- CaBi₂. *Phys. Chem. Chem. Phys.* 2016, 18, 21737-21745.
- (37) Yadav, C. S.; Paulose, P. L. Upper critical field, lower critical field and critical current density of FeTe_{0.60}Se_{0.40} single crystals. *New J. Phys.* 2009, 11, 103046.
- (38) McMillan, W. L. Transition Temperature of Strong-Coupled Superconductors. *Phys. Rev.* 1968, 167, 331-344.
- (39) Wilson, J. A.; Barker, A. S.; Di Salvo F. J.; Ditzenberger, J. A. Infrared properties of the semimetal TiSe₂. *Phys. Rev. B* 1978, 18, 2866-2875.
- (40) Kohn, W. Excitonic Phases. *Phys. Rev. Lett.* 1967, 19, 439-442.
- (41) Helfand, E.; Werthamer, N. R. Temperature and Purity Dependence of the Superconducting Critical Field, H_{c2}. 1964, 13, 686-688.
- (42) Kresin, V. Z.; Wolf, S. A. Fundamentals of superconductivity. Plenum Press, New York and London 1990, 150-153.
- (43) Cao, H. B.; Chakoumakos, B. C.; Chen, X.; Yan, J. Q.; McGuire, M. A.; Yang, H.; Custelcean, R.; Zhou, H. D.; Singh, D. J.; Mandrus, D. Origin of the phase transition in IrTe₂: Structural modulation and local bonding instability. *Phys. Rev. B* 2013, 88, 115122.
- (44) Jobic, S.; Deniard, P.; Brec, R.; Rouxel, J.; Jouanneaux, A.; Fitch, A. N. Crystal and Electronic Band Structure of IrTe₂: Evidence of Anionic Bonds in a CdI₂-like Arrangement. *Z. anorg. allg. Chem.* 1991, 598, 199-215.
- (45) Kohn, W. Image of the Fermi Surface in the Vibration Spectrum of a Metal. *Phys. Rev. Lett.* 1959, 2, 393-394.
- (46) Oda, T.; Shirai, M.; Suzuki, N.; Motizuki, K. Electronic band structure of sulphide spinels CuM₂S₄ (M = Co, Rh, Ir). *J. Phys.: Condens. Matter.* 1995, 7, 4433-4445.
- (47) Lu, Z. W.; Klein, B. M.; Kurnaev, E. Z.; Cherkashenko, V. M.; Galakhov, V. R.; Shamin, S. N.; Yarmoshenko, Yu. M.; Trofimova, V. A.; Uhlenbrock, St.; Neumann, M.; Furubayashi, T.; Hagino, T.; Nagata, S. Electronic structure of CuV₂S₄. *Phys. Rev. B* 1996, 53, 9626-9633.
- (48) Silva-Guillén, J. Á.; Ordejón, P.; Guinea, F.; Canadell, E. Electronic structure of 2H-NbSe₂ single-layers in the CDW state. *2D Mater.* 2016, 3, 035028.
- (49) Kang, Y.-T.; Lu, C.; Yang, F.; Yao, D.-X. Single-orbital realization of high-

temperature s_{\pm} superconductivity in the square-octagon lattice. *Phys. Rev. B* 2019, 99, 184506.

Table 1. Rietveld refinement structural parameters of CuIr₂Te₄. ($a = 3.9397(3)$ Å and $c = 5.3964(6)$ Å)

Label	x	y	z	Site	OCC.
Ir	0.00000	0.00000	0.00000	1a	1.000
Te	0.33330	0.66670	0.2308(4)	2d	1.000
Cu	0.00000	0.00000	0.50000	1b	0.500

Table 2. Comparison of superconducting parameters in AB_2X_4 superconductors

Material	CuIr ₂ Te ₄	CuRh ₂ S ₄	CuRh ₂ Se ₄	Cu _{0.7} Zn _{0.3} Ir ₂ S ₄	CuIr _{1.6} Pt _{0.4} Se ₄	CuV ₂ S ₄
T_c (K)	2.50	4.7	3.5	3.4	1.76	4.45
γ_{exp} (mJ mol ⁻¹ K ⁻²)	10.57	26.9	21.4		16.5	
β_{exp} (mJ mol ⁻¹ K ⁻⁴)	2.15				1.41	
Θ_D (K)	185.5	258	218		212	
$\Delta C/\gamma T_c$	1.82	1.89	1.68		1.58	
$\lambda_{\text{ep(exp.)}}$	0.65	0.66	0.63		0.57	
$N(E_F)_{\text{exp}}$ (states/eV f.u)	2.72				4.45	
$-dH_{c2}/dT$ (T/K)	0.066	0.614	0.181		2.62	
$\mu_0 H_{c2}$ (T)	0.12	2.0	0.44		3.2	
$\mu_0 H^P$ (T)	4.65	8.74	6.51	6.32	3.27	
$\mu_0 H_{c1}$ (T)	0.028					
$\xi_{GL}(0)$ (nm)	52.8			-	0.96	
γ_{cal} (mJ mol ⁻¹ K ⁻²)	6.42					
β_{cal} (mJ mol ⁻¹ K ⁻⁴)	1.77					
$\lambda_{\text{ep(cal.)}}$						
$N(E_F)_{\text{cal}}$ (states/eV f.u)	1.65					
$\Theta_{D,\text{cal}}$ (K)	197.36					

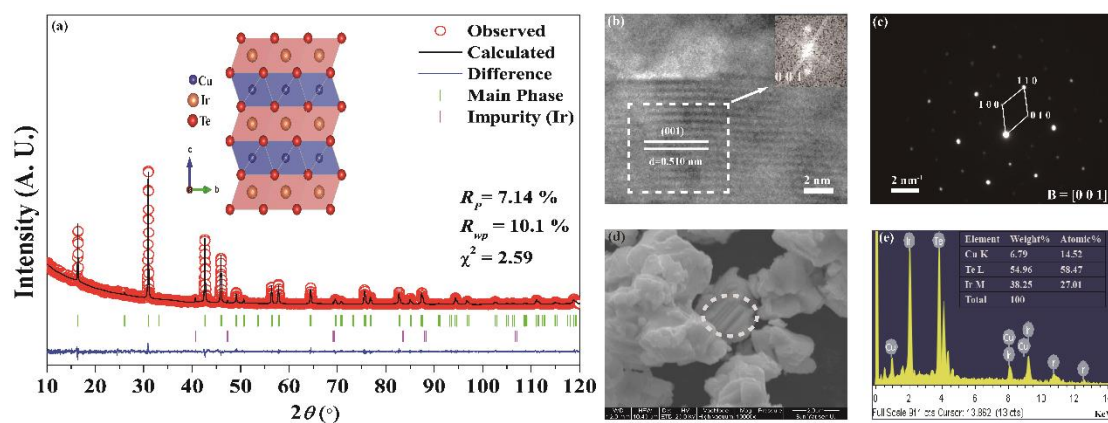


Figure 1. (a) Powder XRD pattern with Rietveld refinement for CuIr_2Te_4 . Inset of (a) shows the view of CuIr_2Te_4 structure along (100) direction. (b) HRTEM image of CuIr_2Te_4 polycrystalline powder. Inset is the corresponding FFT pattern. (c) Selected area (100) direction. (b) HRTEM image of CuIr_2Te_4 polycrystalline powder. Inset is the corresponding FFT pattern. (c) Selected area electron diffraction pattern of CuIr_2Te_4 polycrystalline powder taken on [001] orientation. (d) SEM image of CuIr_2Te_4 polycrystalline powder in the magnification of 13000 times. (e) EDS spectrum and element ratio of CuIr_2Te_4 .

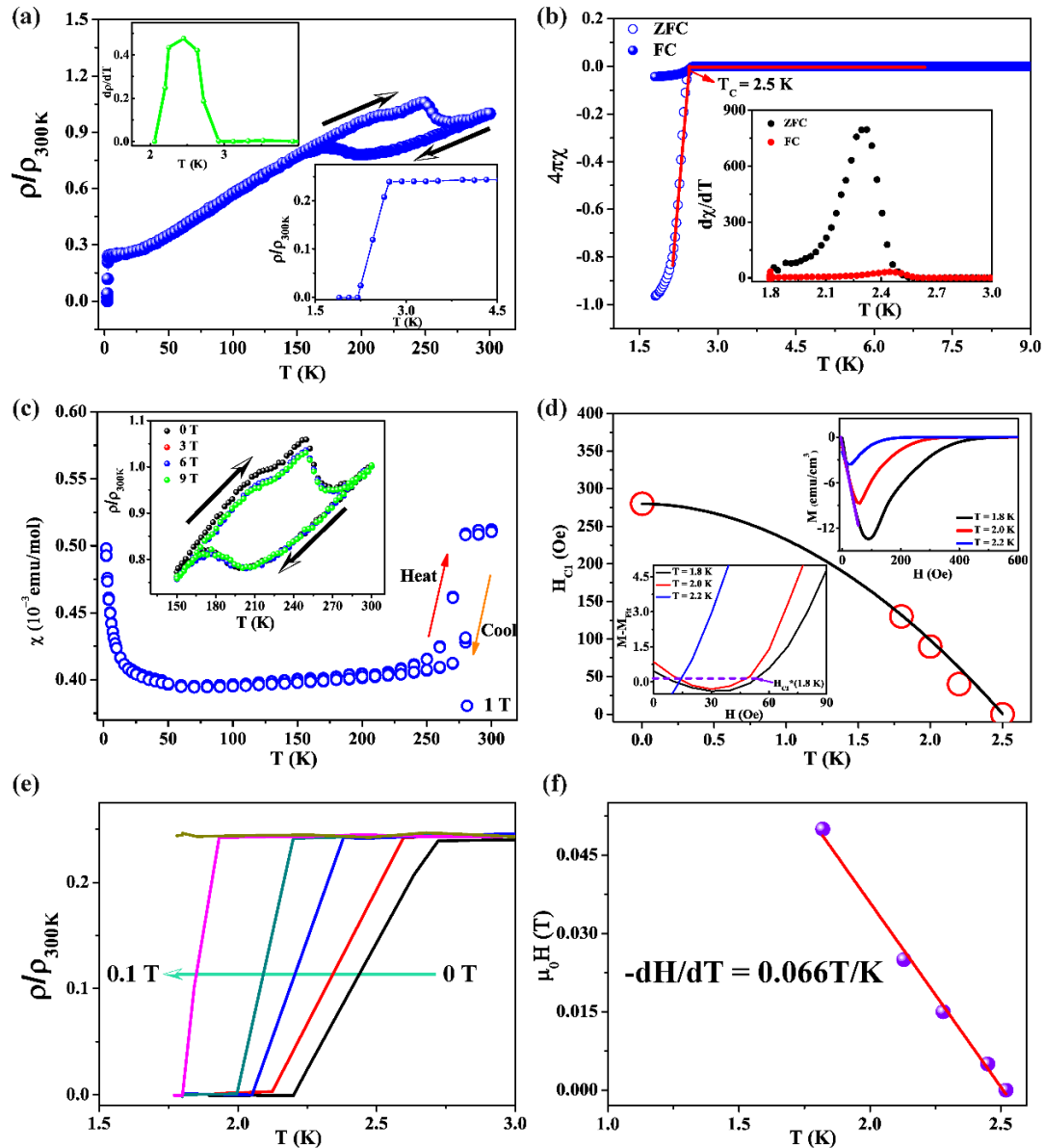


Figure 2. Transport characterization of the normal states and superconducting transitions for CuIr₂Te₄. (a) The temperature dependence electrical resistivity for polycrystalline CuIr₂Te₄. Bottom right corner inset of (a) shows the temperature dependence electrical resistivity at low temperature. Up left corner inset of (a) shows metallic temperature dependence ($d\rho/dT$) in the temperature region of 2 - 5 K. (b) Magnetic susceptibility for CuIr₂Te₄ at the superconducting transitions; applied DC field was 20 Oe. Both zero-field cooling (ZFC) and field cooling (FC, shown more clearly in the inset) curves were measured. Inset of (b) shows the $d\chi/dT$ vs T curve at low temperature. (c) Magnetic susceptibility of CuIr₂Te₄ as a function of temperature at applied field of 1 T. Inset of (c) shows the CDW state at applied fields. (d) Temperature dependence of the lower critical field ($\mu_0 H_{c1}$) for CuIr₂Te₄. Up right corner inset shows magnetic susceptibility at low applied magnetic fields at various applied temperatures for CuIr₂Te₄. Bottom left inset shows $M - M_{fit}$ vs H . (e) Low temperature resistivity at various applied fields for CuIr₂Te₄. (f) $\mu_0 H(T)$ at different T_c s, red solid line shows linearly fitting to the data to estimate $\mu_0 H_{c2}$.

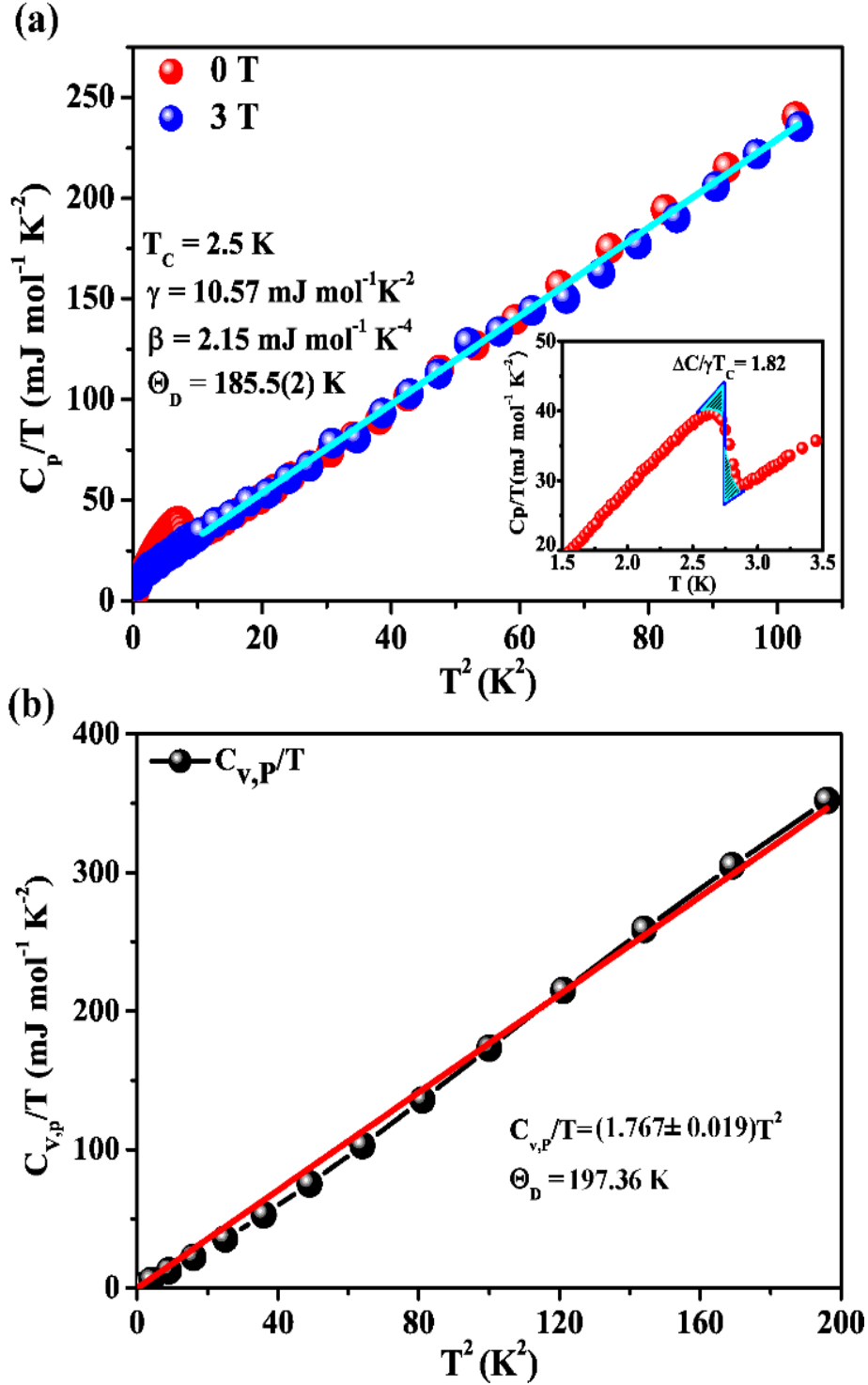


Figure 3. (a) Heat Capacity characterization of CuIr₂Te₄. Debye temperature of CuIr₂Te₄ obtained from fits to data in applied field of 3 T. Inset show heat capacities through the superconducting transitions without applied magnetic field for CuIr₂Te₄. (b) The heat capacity derived from the phonon contribution at low temperature for CuIr₂Te₄.

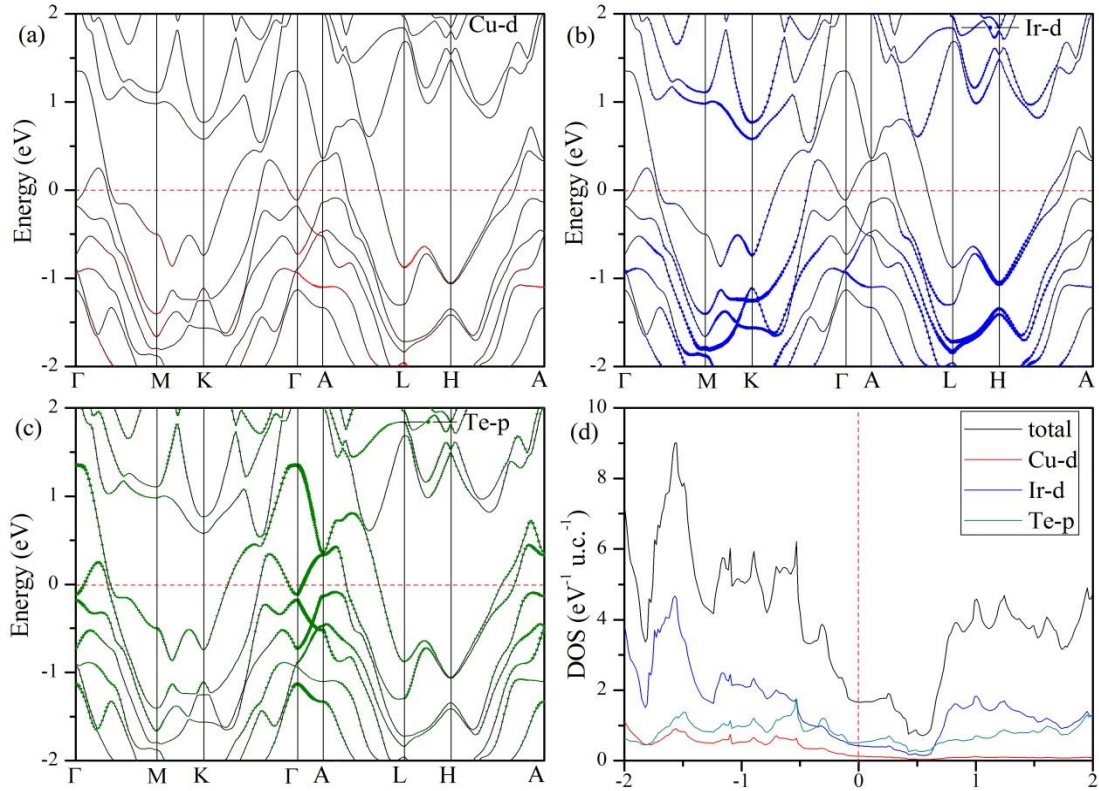


Figure 4. The orbital-projected band structure of CuIr_2Te_4 with SOC projected at (a) Cu d, (b) Ir d and (c) Te p orbitals. The orbital weight at energy eigenvalue E_{nk} is shown by the size of the points. (d) is the total and partial density of states near the Fermi energy.

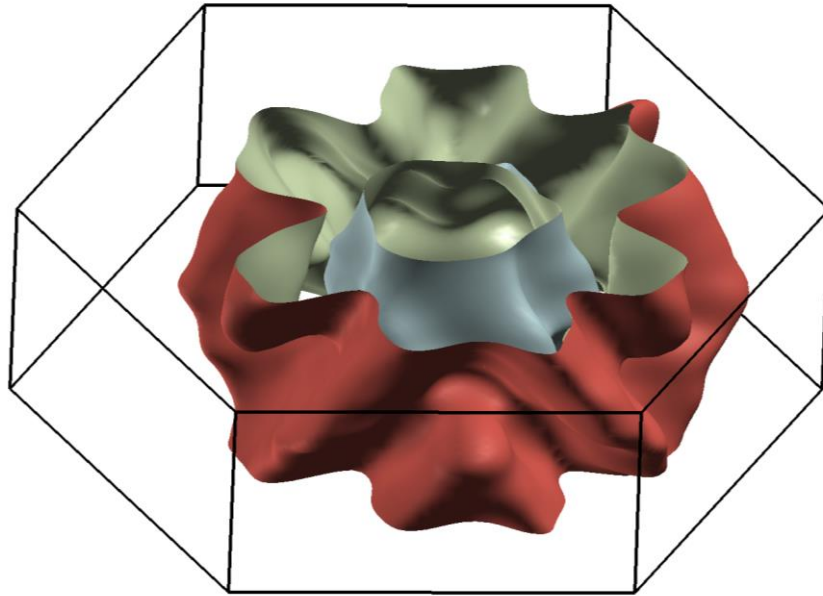


Figure 5. The Fermi surface of CuIr₂Te₄ with SOC.

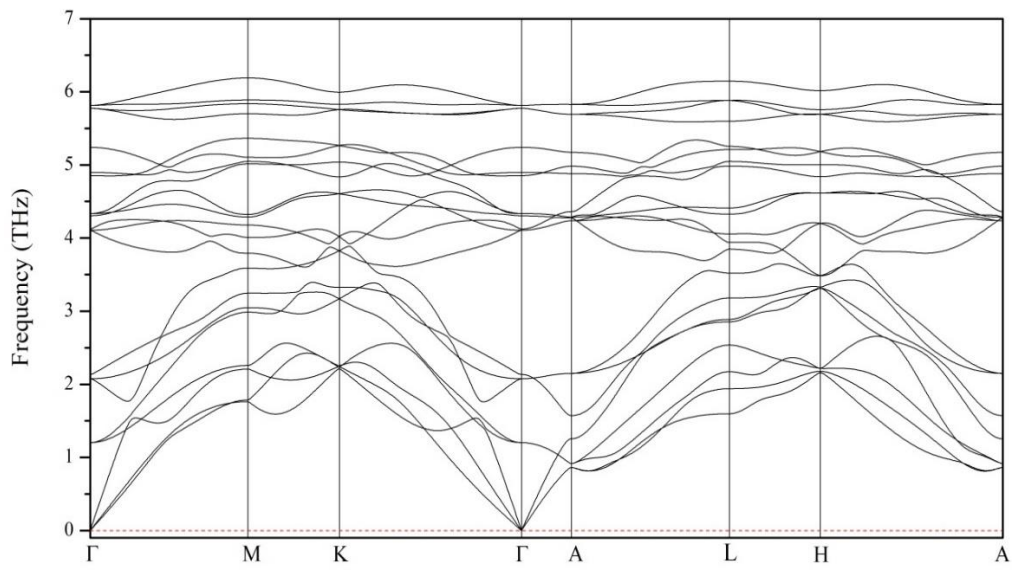


Figure 6. The calculated phonon dispersion of CuIr₂Te₄.